



## Spatial patterns of rainfall and shallow landslide susceptibility

Justin R. Minder,<sup>1</sup> Gerard H. Roe,<sup>2</sup> and David R. Montgomery<sup>2</sup>

Received 24 March 2008; revised 23 September 2008; accepted 3 February 2009; published 22 April 2009.

[1] We quantify the effect of spatial patterns in climatological rainfall on shallow landslide susceptibility by forcing a physically based model of slope stability (SHALSTAB) with the rainfall pattern produced by a high-resolution atmospheric model (MM5) over the western Olympic Mountains of Washington State. Our results suggest that for two small basins in the Olympics, 10 km-scale variations in rainfall have a nontrivial effect on landslide susceptibility. Assuming uniform rainfall equal to the average rainfall over the basins results in a moderate underestimate of landslide susceptibility. Using climatological data from a lowland station to characterize the rainfall over the basins results in a substantial underestimate of susceptibility. The effect of spatial variability in rainfall on variations in stability is comparable to the effect of moderate-to-large variability in soil parameters (such as  $\pm 30\%$  variations in soil thickness). At a practical level, these results imply that accounting for persistent patterns of rainfall may aid in discerning regions within the same watershed where similar land use practices will lead to differing landslide risk.

**Citation:** Minder, J. R., G. H. Roe, and D. R. Montgomery (2009), Spatial patterns of rainfall and shallow landslide susceptibility, *Water Resour. Res.*, 45, W04419, doi:10.1029/2008WR007027.

### 1. Introduction and Background

[2] One of the primary triggers for shallow landslides on soil mantled landscapes is high-intensity and/or long-duration rainfall [e.g., Caine, 1980; Guzzetti *et al.*, 2008]. Over mountainous regions, where slides tend to occur, atmospheric circulations forced by the topography lead to distinct rainfall patterns that may include greater than twofold differences in accumulation over horizontal distances of a few kilometers [e.g., Bergeron, 1968; Smith *et al.*, 2003; Roe, 2005; Kirshbaum and Durrant, 2005]. However, it is not generally known how strongly such spatial variations of rainfall control slope stability. If the influence is sizable, and the rainfall patterns are predictable, then climatologies and/or forecasts of kilometer-scale rainfall patterns may prove valuable for landslide hazard assessment and forecasting.

[3] In this paper we will distinguish between different time scales on which rainfall characteristics affect the spatially variable likelihood of landslide occurrence over a region. Landslide probability on storm time scales will refer to the likelihood of slope failure during a single storm or series of storms that may last from hours to weeks. This may be strongly influenced by the detailed features of a given storm such as its intensity, duration, track, structure, and interaction with the topography. This contrasts with landslide susceptibility on climatological time scales, which

will refer to the spatially variable likelihood of failure given the distribution of storms that occur in a region over the course of years to millennia. This depends on the statistical properties of the climatological distribution of storms, including the average, variability, and extremes of storm intensity, duration, etc.

[4] Previous work on rainfall patterns and slope stability is limited and almost exclusively has focused on the storm time scale. Some of these studies have used slope aspect and wind direction in an attempt to empirically relate the pattern of wind driven rainfall to the locations of slope failures [e.g., Pike and Sobieszczyk, 2008], but these studies typically neglect horizontal variations in rainfall rate (the vertical flux of rain), variations which, as mentioned above, can be quite large. Recently researchers have begun to use small-scale rainfall patterns in modeling slides triggered by individual storms. In New Zealand a landslide forecasting system is being developed using physically based models of hydrology and slope stability forced by rainfall from a numerical weather prediction model on a 12 km horizontal grid [Schmidt *et al.*, 2008]. However, while small-scale rainfall forecasts have been used in this modeling efforts, the authors stopped short of quantifying the effect of the spatial rainfall variations or the value added to their predictions by considering them.

[5] Other studies have used ground- and space-based radar measurements to estimate the rainfall distribution and relate it to slide locations [Campbell, 1975; Wieczorek *et al.*, 2001; MacLeod, 2006; Chang *et al.*, 2008]. Uncertainties with estimating surface rainfall from radar can limit the effectiveness of such methods [e.g., Wieczorek *et al.*, 2001; MacLeod, 2006], however a combination of radar and gauge observations can be used to make a more confident analysis of the rainfall pattern [e.g., Chang *et al.*, 2008].

<sup>1</sup>Department of Atmospheric Science, University of Washington, Seattle, Washington, USA.

<sup>2</sup>Department of Earth and Space Sciences, University of Washington, Seattle, Washington, USA.

Using NEXRAD radar *Wieczorek et al.* [2001] found that a localized ( $\sim 5$  km radius) region of particularly heavy rainfall was collocated with many of the slope failures occurring during an extreme convective storm on 27 June 1995 in the Blue Ridge Mountains of Madison County, Virginia. Using a physically based transient model of slope stability forced by radar-derived rainfall from this event, *Morrissey et al.* [2004, p. 294] found significant “spatial and temporal variations of the factor of safety” (a measure of slope instability) correlated with the movement of individual convective storm cells, just a few kilometers in width, across the landscape. Results from this event suggest an important role for small-scale rainfall features in determining where slides are triggered on the storm time scale. Yet, if the rainfall from such convective cells is distributed randomly across a region from storm to storm they will have no net influence on the pattern of susceptibility over climatological time scales. For spatial variations in mountain rainfall to influence the climatological pattern of landslide susceptibility they must be both large and persistent enough. Whether this is the case on small (10 km or less) scales remains an open question.

[6] In mapping landslide susceptibility over climatological time scales, spatial distributions of various parameters (e.g., slope, drainage area, vegetation, bedrock geology) are often used. Quantitative hazard assessment is typically accomplished either through the use of empirical models [e.g., *Gupta and Joshi*, 1990; *Baeza and Corominas*, 2001; *Lee et al.*, 2003; *Saha et al.*, 2005], or spatially distributed physically based models of slope stability and hydrology [e.g., *Montgomery and Dietrich*, 1994; *Wu and Sidle*, 1995; *Casadel et al.*, 2003; *Morrissey et al.*, 2004]. Information on 10 km-scale spatial variability of rainfall is very seldom considered in long-term susceptibility analysis, in part because mountain rainfall patterns have not been well observed or understood on those scales. However, in recent years it has become clear that large variations in precipitation occurring on spatial scales of 10 km or less are a persistent and predictable feature of mountain climates in a variety of regions [*James and Houze*, 2005; *Anders et al.*, 2006, 2007; *Minder et al.*, 2008]. A better understanding of the impact of these variations may have important applications. For instance, researchers have been developing techniques to use intensity-duration thresholds for slope failure, and satellite-borne radar estimates of precipitation at  $0.25^\circ \times 0.25^\circ$  horizontal resolution to issue near real-time assessment of landslide hazard [*Hong et al.*, 2006]. However, the effects of subgrid-scale variations in rainfall on such a system have not been determined. Furthermore, observations of precipitation in mountainous regions are usually sparse. As a result, studies of landslides often are forced to rely upon gauge observations from a single point to characterize the rainfall over an entire study region (e.g., *Casadel et al.* [2003] and *Gorsevski et al.* [2006] provide recent examples). Available gauges tend to be sited in accessible lowlands and valleys [*Groisman and Legates*, 1994], locations that may poorly represent conditions at the locations where slides occur. Yet the errors in hazard assessments due to the distance between gauge observations and landslide locations have not been well quantified.

[7] We aim to better characterize the influence of small-scale rainfall patterns on climatological shallow landslide

susceptibility. To do so we consider two adjacent watersheds in the Olympic Mountains of Washington State and use a modeled rainfall climatology (supported by observations) to force a simple model of slope stability in order to address the following: What effect on landslide susceptibility may be expected from rainfall variations occurring over spatial scales of 10 km? How large of a bias in hazard assessment may occur if a lowland station is used to characterize precipitation across a mountainous catchment? How does spatial variability of precipitation compare to spatial variability of soil properties for determining variations in slope stability?

## 2. Rainfall and Landslides Over the Western Olympic Mountains

[8] The Olympic Mountains of Washington State receive copious amounts of precipitation over their western (windward) slopes. Most of this rainfall occurs during midlatitude cyclones as stably stratified moist air from over the Pacific is forced over the topography by southwesterly winds. Precipitation at locations in the Olympics can amount to over 5 m in the annual total. A small-scale precipitation climatology was developed over the Olympics by *Anders et al.* [2007] using 6 years of forecasts from the MM5, a high-resolution (4 km in the horizontal) weather model used for operational forecasts in the Pacific Northwest (<http://www.atmos.washington.edu/mm5rt/mm5info.html>) [*Mass et al.*, 2003]. This climatology suggests that substantial enhancement of storm total and annual mean precipitation occurs over 10–20 km-scale ridges relative to the adjacent valleys [*Anders et al.*, 2007; *Minder et al.*, 2008]. The most pronounced enhancement in the model occurs over a 15 km wide, 1 km high topographic ridge separating the Queets and Quinault basins (Figure 1 shows the topography of these basins).

[9] Four years of observations from a high-density network of precipitation gauges in the region support the model climatology, with MM5 and gauges both showing 60–80% more rainy season (October–May) precipitation atop the ridge than in the valleys that flank it. Figure 2 shows a comparison of annual total precipitation from the MM5 and observations at gauge locations in a transect across the ridge for most of one rainy season (locations of the gauges are shown in Figure 3). The model captures well both the amount and spatial distribution of precipitation across the gauge network, with the model’s normalized route mean squared error in rainy season total precipitation at the gauge sites ranging from 10–22% [*Minder et al.*, 2008]. Favorable performance of the MM5 is found despite the coarseness of its 4 km mesh relative to the ridge valley topography, and MM5 case studies with higher (1.33 km) resolution produce similar rainfall [*Minder et al.*, 2008]. The pattern of ridge top enhancement is a particularly robust feature of heavy rainfall events [*Minder et al.*, 2008], during which the ridge can receive over three times the rainfall of adjacent valleys [*Anders et al.*, 2007]. While individual major storms are frequently misforecast by the model, on average the precipitation modeled for major storms is quite realistic [*Anders et al.*, 2007; *Minder et al.*, 2008].

[10] Shallow landslides are a pervasive feature in the western Olympic Mountains. Mapped shallow and deep-seated landslides in the Queets and Quinault basins are

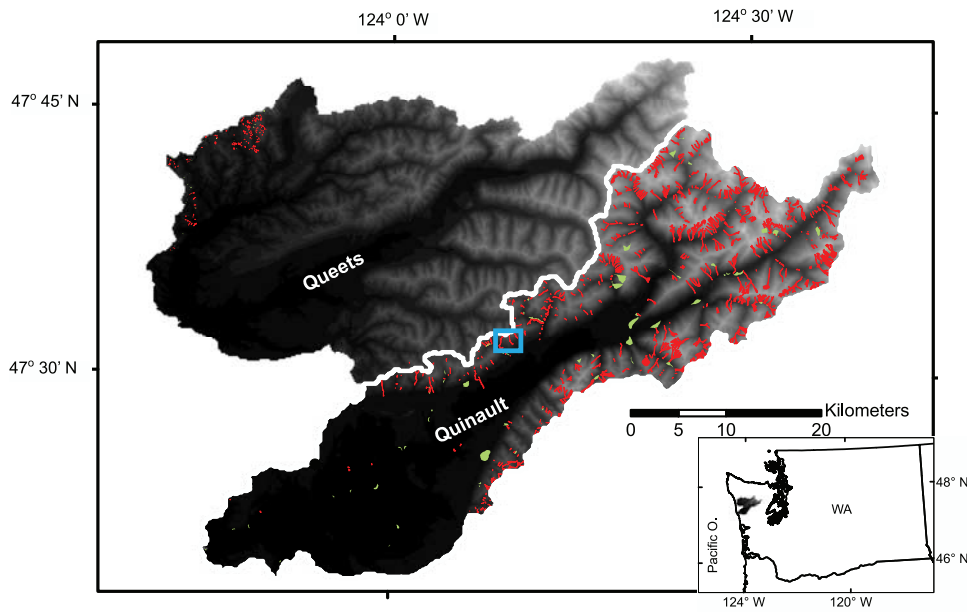


**Figure 1.** Topography and mapped slides for the Queets and Quinault basins (location of the basins within Washington State is shown in inset map). Elevation is shaded in gray scale and ranges from 0 to 2.2 km. Shallow slides are shown in red, and deep-seated slides are green. Mapped slides include scar and runoff, and complete mapping has only been done for the Quinault basin. The white line indicates the divide between the two basins. The blue box indicates the location of Figure 6.

shown in Figure 1. These were primarily surveyed by *Lingley* [1999] using aerial photography and made available as a digital coverage by the Washington State Department of Natural Resources Landslide Hazard Zonation Project (<http://www.dnr.wa.gov/forestpractices/lhzproject/>). This region has a variety of land cover, with vegetation ranging from mature forest (> 50 years old) to clear cuts. The surface geology is also variable, including Quaternary alpine glacial deposits as well as Tertiary marine sedimentary and volcanoclastic rocks (broken by a number of faults, shearing, and bedding structures) [*Lingley*, 1999].

### 3. Methods

[11] We wish to quantify the effect that spatial variations in climatological precipitation may have on shallow landslide susceptibility. To this end we will use the rainfall pattern from the MM5 as a best estimate of the rainfall distribution over the region, and the SHALSTAB model of slope stability [*Montgomery and Dietrich*, 1994] as a representation of the fundamental physics governing landslide triggering by rainfall. Our aim is to determine, in a semi-idealized context, if climatological rainfall patterns similar to those found in the Olympic mountains represent a large enough physical signal to play an important role in determining landslide susceptibility. It is not our intent to directly test whether considering rainfall patterns improves prediction of landslide locations, as uncertainties in our data sets (e.g., rainfall climatology, landslide mapping, and soil properties) make such a task intractable.

[12] The SHALSTAB model [*Montgomery and Dietrich*, 1994], utilizes GIS software to couple an “infinite slope” stability model with a steady state model of rainfall infiltration and topographic-driven flow of water within the soil. The only detailed spatial information required by the model is a high-resolution digital elevation model (DEM)

of the topography. By assigning spatially uniform mean values to other, often poorly mapped, parameters the model can be used to indicate where topographic factors make slopes prone to failure, with steep, convergent slopes identified as the most unstable [*Montgomery and Dietrich*, 1994]. Since root strength offers significant reinforcement in forested regions, we consider a formulation of SHALSTAB that includes the effective soil cohesion due to vegetation [*Montgomery et al.*, 2000]. However to avoid making assumptions about landslide size we consider only basal

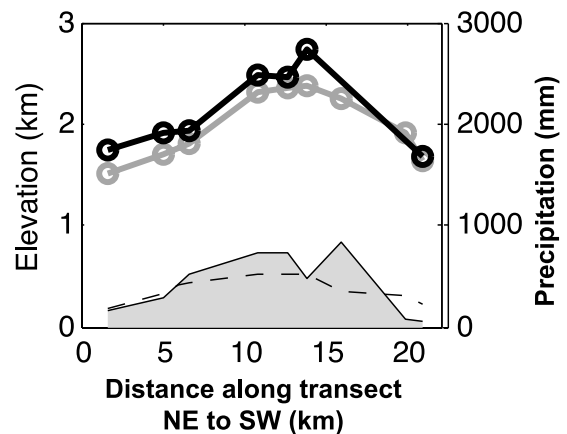


**Figure 2.** Total modeled and observed precipitation at locations along the transect of gauges shown in Figure 3 for November–April 2004–2005. Elevations of gauge sites are shown by the shaded terrain profile (the model elevations interpolated to the gauge sites are shown with the dashed line). Gauge observation are shown in black, and model climatology interpolated to gauge locations is shown in gray (adapted from *Minder et al.* [2008] and reproduced with permission of Wiley-Blackwell).

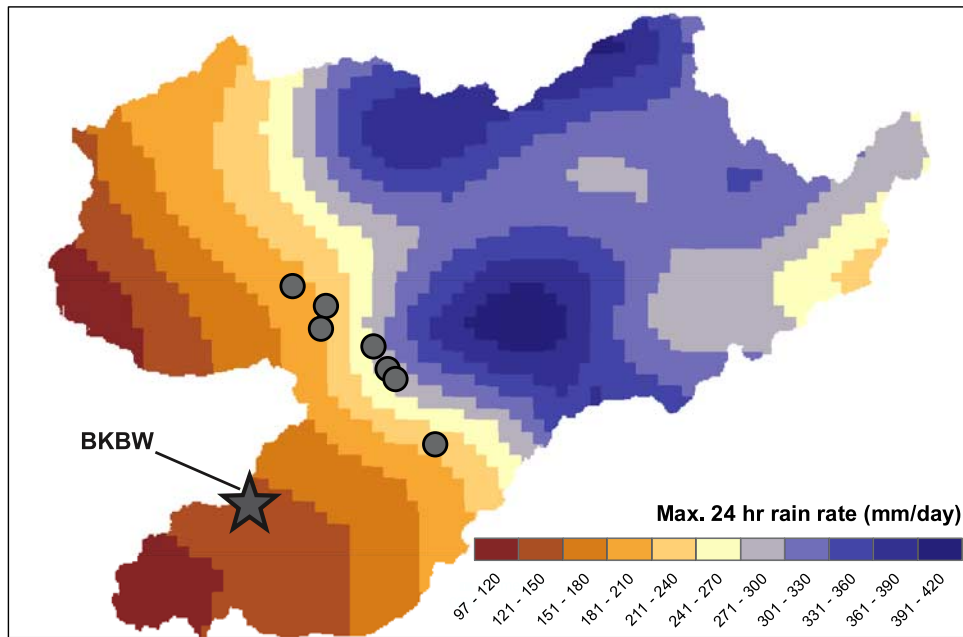


**Figure 3.** Maximum 24 h averaged rainfall rate from 7 years of MM5 high-resolution atmospheric model iterations (reinterpolated from the 4 km MM5 grid to 1 km). The location of the Black Knob weather station (BKBW) is indicated with a star, and the location of the gauge network of *Anders et al.* [2007] and *Minder et al.* [2008] is shown with circles.

cohesion and not cohesion around the perimeter of the slide. SHALSTAB may be applied by solving, at each DEM grid cell, for the critical value of a chosen parameter at which failure should occur. In principle any parameter may be used. We choose to solve for critical soil cohesion ( $C_{crit}$ ) as our measure of slope instability:

$$C_{crit} = z\rho_w g \cos^2(\theta) \tan(\phi) \times \left[ \frac{a}{b} \frac{q}{T \sin(\theta)} - \frac{\rho_s}{\rho_w} \left( 1 - \frac{\tan(\theta)}{\tan(\phi)} \right) \right], \quad (1)$$

where  $q$  is a steady state precipitation flux,  $g$  the acceleration due to gravity,  $T$  is the saturated soil transmissivity,  $a/b$  is the contributing drainage area per grid cell length (calculated as done by *Montgomery et al.* [2000]),  $\rho_s$  is the wet bulk density of the soil,  $\rho_w$  is the density of water,  $\theta$  is the angle of the topographic slope,  $\phi$  is the angle of internal friction, and  $z$  is the soil depth. Actual soil cohesion likely varies greatly across our study area because of variations in vegetation and land use, however solving for  $C_{crit}$  means we need not make assumptions about the actual cohesion. Note that in the model slopes that become saturated have their critical cohesion set to the value occurring at saturation, as excess water is assumed to run off as overland flow. For given topography and soil parameters, locations predicted to remain stable under saturated conditions, even without soil cohesion, are termed “unconditionally stable.”

[13] In our SHALSTAB simulations we use a 10 m DEM grid, the highest resolution available for our study area. To isolate the effects of spatial variability in rainfall we assume uniform values for soil depth and material properties (Table 1). These values were mostly taken from previous studies in the Oregon Coast Range (e.g., *Montgomery et al.*, 2000), and are only meant to represent reasonable mean values for illustration.

[14] SHALSTAB models the response of soil pore pressures to steady rainfall of infinite duration. This is an approximation to the pseudo steady state response of actual soils to prolonged rainfall, which occurs on a time scale of about 1 day for small slides in diffusive soils [*Iverson*, 2000]. Many slides are actually triggered by the transient response of pore pressures to bursts of intense rainfall, which occurs on a time scale of tens of minutes for shallow slides in diffusive soils [*Iverson*, 2000]. However, we focus on the pseudo steady response since it is less dependent upon high-frequency variations in rain rate (which are poorly characterized), and since regions of increased saturation due to this slow response will be more prone to failure due to transient forcing.

[15] We first run SHALSTAB to calculate the critical cohesion using equation (1), including the spatially varying pattern of rainfall ( $q(x, y)$ ) predicted by MM5. For this we use the 7 year maximum 24 h average rainfall rate at each MM5 grid point (Figure 3). The 7 year maximum rainfall rate is used to determine the most hazardous conditions at each location that would be expected over a climatological time scale. Ideally a period longer than 7 years would be used to develop a proper rainfall climatology, but we are limited by the extent of the MM5 data set and the semi-

**Table 1.** Uniform Values for Soil Parameters Used in SHALSTAB Modeling

Parameter <sup>a</sup>	Value
$\rho_w/\rho_s$	2
$z$	1 m
$\phi$	33°
$T$	65 m <sup>2</sup> /d

<sup>a</sup>Parameters are defined in text.

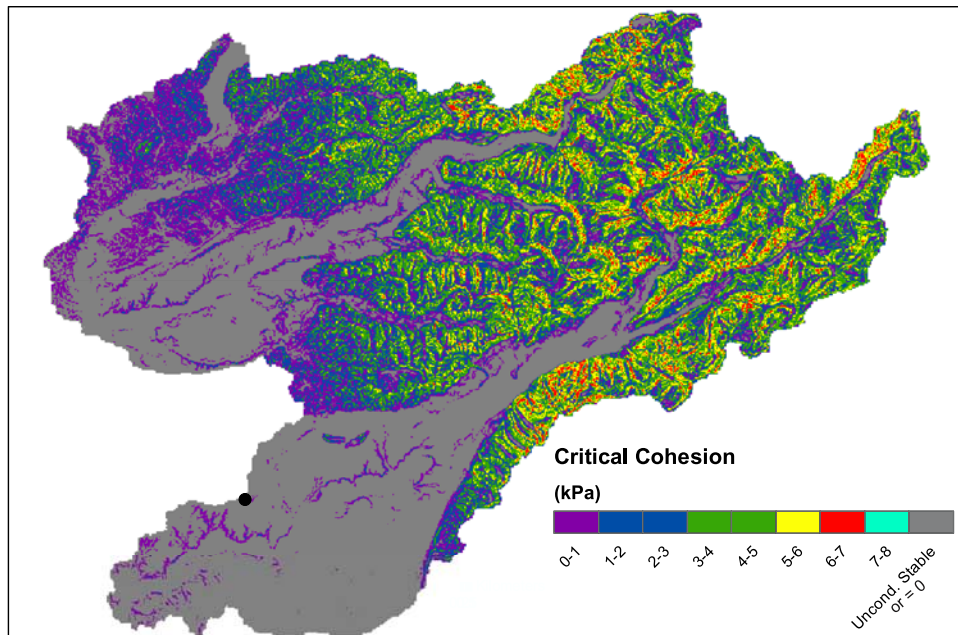


**Figure 4.** Critical cohesion as predicted by SHALSTAB (equation (1)) using the MM5 rainfall climatology shown in Figure 3. Gray areas represent locations classified as unconditionally stable or with  $C_{crit} = 0$ .

idealized nature of our study only requires a plausible climatology. Furthermore, on the basis of the storm-to-storm robustness of the rainfall pattern we expect a longer climatology would look similar, except perhaps with larger extreme rainfall rates. A 24 h averaging period is used since this is the time scale over which pseudo steady state adjustment of groundwater flow occurs [Iverson, 2000]. To calculate the 24 h rain rates we first construct a time series of 0000–1200 UTC and 1200–2400 UTC forecast rainfall from forecast hours 24–36 of the MM5 runs (initialized twice daily at 0000 and 1200 UTC). For practical reasons the 24 h averages are obtained by using a 24 h running mean window that shifts forward in time by 12 h increments rather than by 1 h increments, thus the actual maximum rate is potentially underestimated. Before feeding the rainfall pattern into SHALSTAB we linearly reinterpolate it to a 1 km grid to smooth out some of the sharpest gradients introduced by the coarseness of the MM5 mesh.

[16] The pattern of 24 h maximum rainfall rate shown in Figure 3 exhibits both a steady increase in rainfall toward the interior of the Olympic mountains, as well as variations in rainfall associated with the major ridges and valleys. This pattern is somewhat different than the pattern of rainy season total precipitation (shown with the transect in Figure 2 and that of Anders *et al.* [2007] and Minder *et al.* [2008]). While both the season total and extreme rainfall patterns exhibit large variations associated with the ridge valley relief, for the extreme rainfall the maximum appears to be shifted away from the ridge crest toward the southeastern slopes of the ridge. Case studies analyzed by Minder *et al.* [2008] suggest that such a shift in the rainfall pattern is reasonable.

[17] We consider the results from our first SHALSTAB simulation, using the MM5 rainfall pattern, as our best estimate of the true slope stability. We then rerun SHALSTAB twice, both times with uniform rainfall forcing. For the first

of these runs we choose an uniform rain rate representative of the spatially averaged maximum 24 h rain rate over the basins: 256 mm/d. Comparison of the output from this run with the original patterned rainfall run is used to determine how much the rainfall pattern affects landslide susceptibility. For the second run we use the MM5 rainfall to choose a uniform rain rate representative of the maximum 24 h value that would be measured at the location of the Black Knob (BKBW, shown in Figure 3), the nearest weather station with precipitation data for multiple years that would be readily available for hazard assessment: 141 mm/d. Comparison of the output from this run with the patterned rainfall run is used to determine the biases that may occur if lowland observations are used to characterize the rainfall and landslide susceptibility across a mountainous catchment.

#### 4. Results

[18] Figure 4 shows  $C_{crit}$  calculated across the basin using the MM5 precipitation pattern. The highest values of critical cohesion are greater than 6 kPa, suggesting that those slopes would fail under the most extreme 7 year rainfall unless they had significant stabilization associated with vegetation and root strength. Many of the mapped slides initiate in steep topographic hollows, and SHALSTAB does qualitatively well at identifying these locations as regions of high  $C_{crit}$  (e.g., Figure 5). We make a cursory check on the ability of SHALSTAB to identify the locations prone to failure using methods analogous to Montgomery *et al.* [1998]. More specifically, for each of the shallow landslides mapped in Figure 1 we associate the slide with the location within the mapped slide polygon where the critical cohesion is a maximum (this is done to better associate the mapped slide, which include both scar and runout, with the location of failure). We bin the frequency of slide occurrence by the

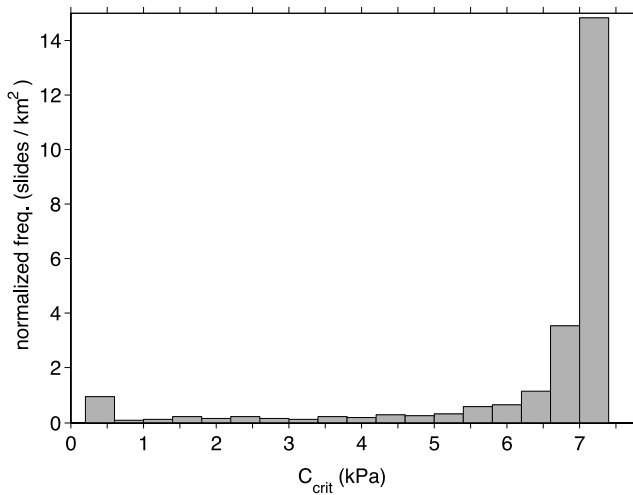


**Figure 5.** Number of mapped landslides per square kilometer in each  $C_{crit}$  category (calculated as described in text) for slides mapped in the Queets and Quinault basins and SHALSTAB-calculated values of  $C_{crit}$ .

slide's maximum critical cohesion, and then normalize each bin by the total area in the study region with that value of critical cohesion. The results from this, plotted in Figure 6, show a clear tendency for slides to occur much more frequently with high values of  $C_{crit}$ , as should be expected if the model is skillful at identifying the locations where failures tend to occur. While this analysis does not definitively demonstrate SHALSTAB's skill, the combination of these results with more rigorous evaluations of the model in settings similar to our study region [e.g., *Montgomery et al.*, 1998] give us confidence in its appropriateness for this study.

[19] Figure 7 shows the difference in  $C_{crit}$  that occurs when patterned rainfall is used relative to when uniform rainfall equal to the region average is used. As should be expected, it shows that neglecting the rainfall pattern causes an overestimate (underestimate) of slope stability in regions that receive more (less) than the area average rainfall. The change in  $C_{crit}$  is modest over most of the study region ( $< 0.5$  kPa), but can be more substantial near the locations of the minima and maxima in the precipitation pattern ( $> 1$  kPa). A larger fraction of the study region experiences an overestimate than an underestimate of the stability when the pattern is neglected since the most gentle slopes, which are unconditionally stable, tend to reside in the lowlands and valleys where rainfall rates tend to be more modest.

[20] Figure 8 shows the difference in  $C_{crit}$  that occurs when patterned rainfall is used relative to when uniform rainfall from the lowland station BKBW is used (patterned lowland). Since nearly all locations where slides may occur (locations that are not unconditionally stable) receive more rainfall than the BKBW's lowland location,  $C_{crit}$  is found to increase, and the stability is overestimated, almost everywhere when the rainfall pattern is considered, and by upward of 3 kPa in the center of the ridge's rainfall maximum. In other words, considering the rainfall pattern instead of just the lowland precipitation reveals a larger number of slopes that require significant reinforcement from root strength to resist failure.

[21] We further analyze the results of these experiments by considering bulk statistics from the runs. Figure 9a shows a frequency distribution of  $C_{crit}$  values for the patterned and uniform rainfall cases. When the rainfall pattern is neglected in favor of the average rainfall, the distribution of  $C_{crit}$  is shifted toward somewhat lower (more stable) values, corresponding to an overall modest overestimate of the

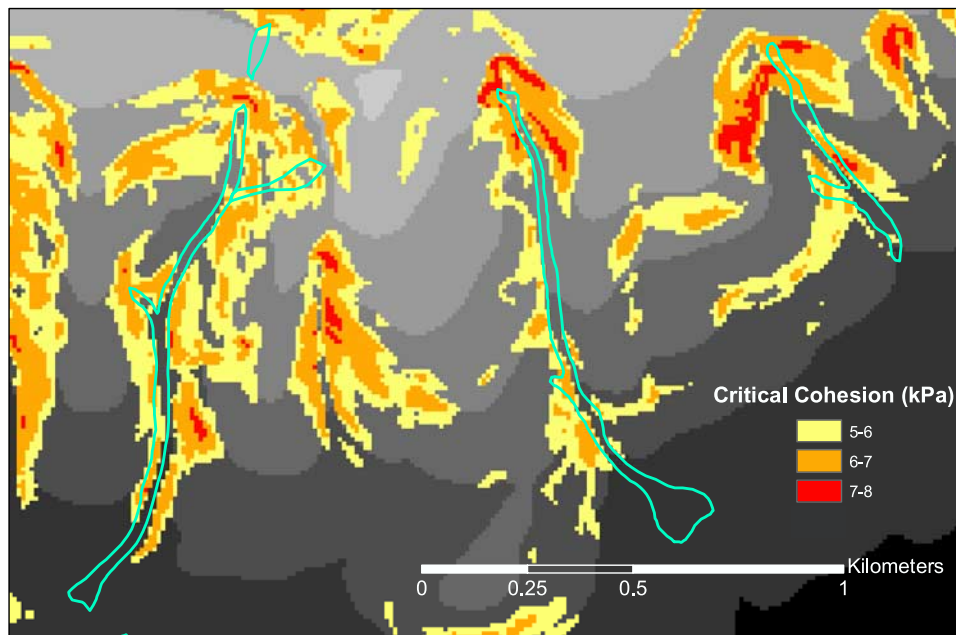


**Figure 6.** Mapped slides and SHALSTAB modeled  $C_{crit}$  for the individual hillsides indicated by the blue box in Figure 1. Elevation is shown with gray-scale shading (shading interval of 100 m). Regions of high  $C_{crit}$  are color shaded according to the inset key. The perimeters of several mapped slides are delineated in cyan.

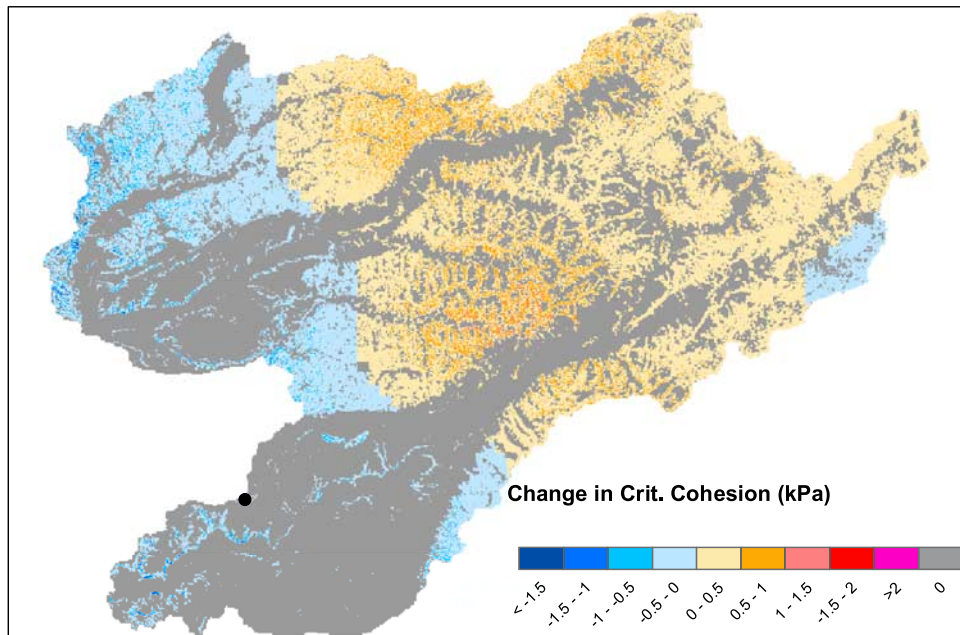


**Figure 7.** Change in SHALSTAB critical cohesion ( $C_{crit}$ ) when using the MM5 rainfall pattern relative to uniform average precipitation. This is calculated by subtracting the  $C_{crit}$  attained from the simulation with uniform precipitation equal to the region average MM5 precipitation from the  $C_{crit}$  attained when using the MM5 rainfall pattern.

stability of slopes in the study region. When the rainfall pattern is neglected in favor of the lowland rainfall a much more substantial shift in the distribution and overestimate of the stability occurs.

[22] Figure 9b shows the frequency distribution of the changes in critical cohesion experienced between the uniform and patterned case. Figure 9b again shows that using the rainfall pattern instead of the uniform average precipitation increases  $C_{crit}$  for some slopes and decreases it for

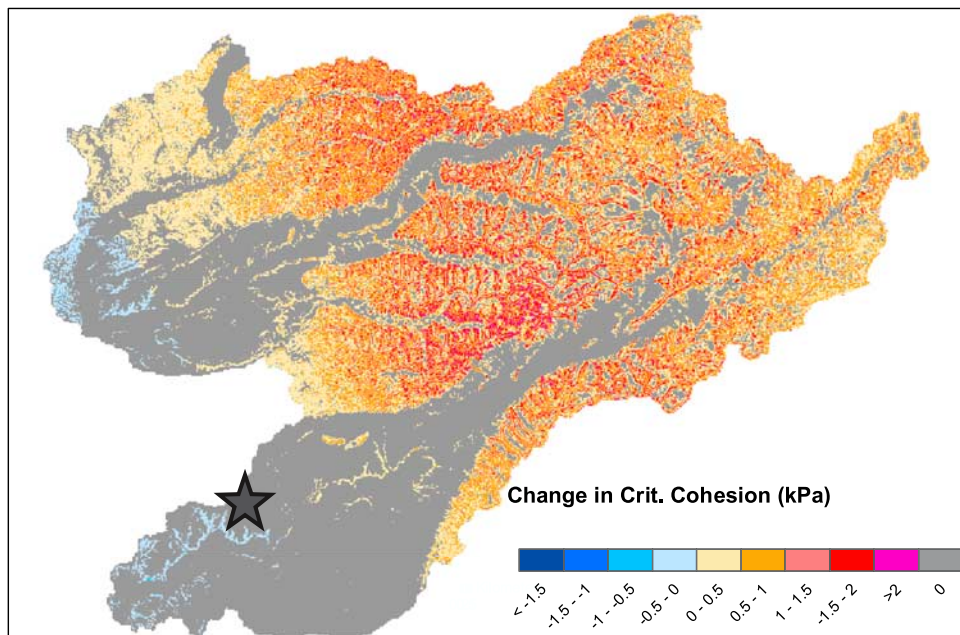


**Figure 8.** Change in SHALSTAB critical cohesion ( $C_{crit}$ ) when using the MM5 rainfall pattern relative to uniform lowland precipitation. This is calculated by subtracting the  $C_{crit}$  attained from the simulation with uniform precipitation equal to the MM5 precipitation at the site of the lowland BKBW station from the  $C_{crit}$  attained when using the MM5 rainfall pattern.

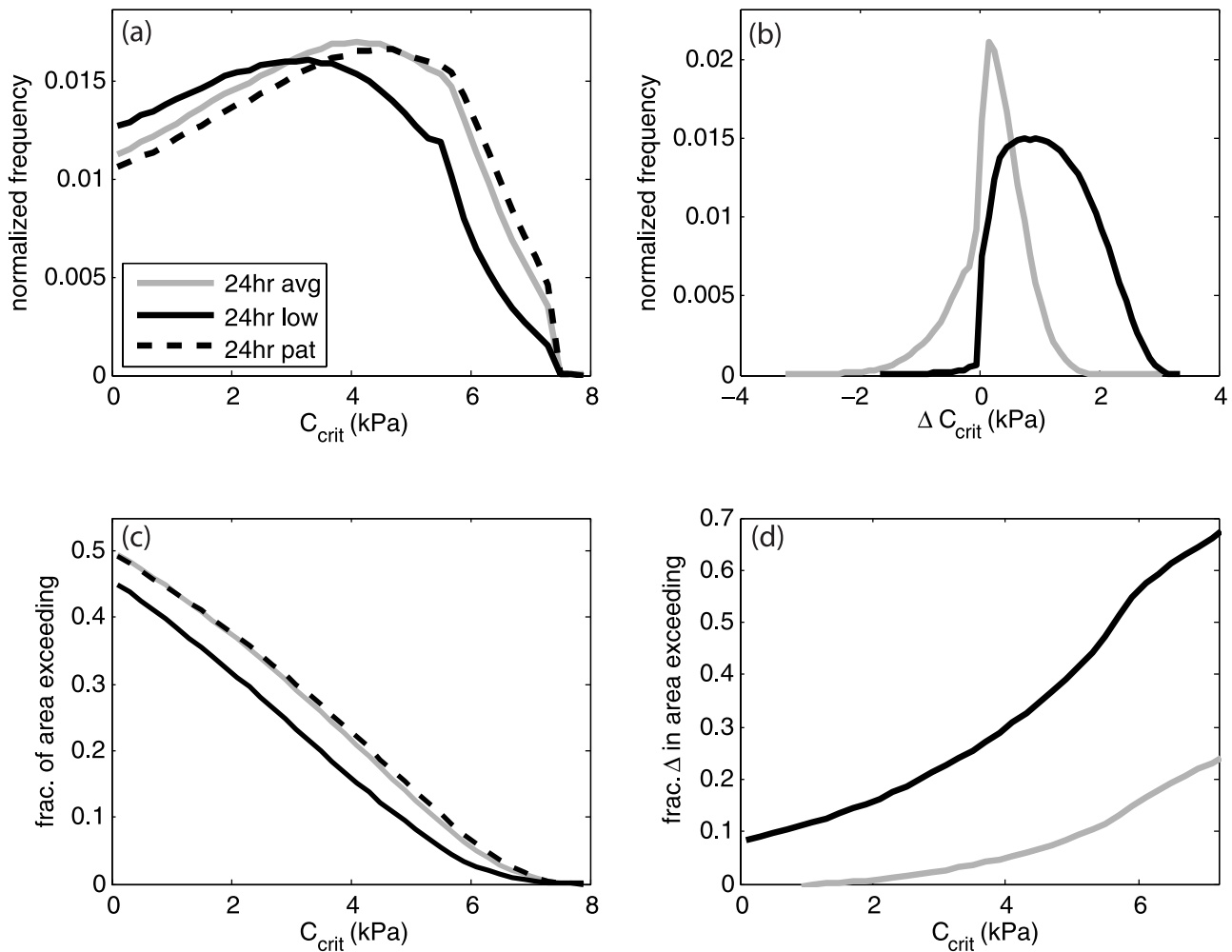


**Figure 9.** (a) Frequency distribution of  $C_{crit}$  for SHALSTAB runs with MM5 patterned rainfall (dashed black line), uniform region average rainfall (solid gray line), and lowland rainfall (solid black line). The distributions have been normalized by the total area of the basins, and cells with  $C_{crit} = 0$  are omitted. (b) Frequency distribution of changes in  $C_{crit}$  between the run with patterned and the runs with uniform rainfall (gray line for uniform average rainfall, black line for uniform lowland rainfall). Distributions have been normalized as in Figure 9a, and cells with change in  $C_{crit} = 0$  are omitted. (c) Fractional area of the region exceeding various values of  $C_{crit}$  for patterned and uniform rainfall runs (line styles as in Figure 9a). (d) Fractional change in area exceeding various values of  $C_{crit}$  between SHALSTAB runs with patterned and uniform rainfall (line styles as in Figure 9b).

others, indicating that neglecting rainfall patterns under or over estimates the stability depending upon location. In contrast, using the rainfall pattern instead of the uniform lowland precipitation increases  $C_{crit}$  nearly everywhere, indicating that uniform lowland rainfall results in a very widespread overprediction of slope stability.

[23] The scale of the differences in  $C_{crit}$  can be used to place the impact of spatial rainfall variations in context. For instance, direct measurements of cohesive reinforcement by roots in Pacific Northwest forests (collected from the Oregon Coast Range) reveal that typical cohesion from roots ranges from 6.8 to 23.2 kPa for industrial forests, and from 1.5 to 6.7 kPa for clear cuts <11 years old [Schmidt *et al.*, 2001]. Therefore, particularly for heavily logged basins, the maximum biases in the estimate of  $C_{crit}$  due to use of uniform lowland rainfall ( $\sim 3$  kPa) are equiv-

alent to a substantial portion of the net reinforcement provided by tree roots, suggesting that such biases are indeed relevant. Even the seemingly modest changes in the estimate of  $C_{crit}$  introduced by using uniform averaged precipitation (as much as 1 kPa) may appear nontrivial in this context.

[24] Figure 9c shows the fractional area of the landscape exceeding various values of  $C_{crit}$ . This can be used to determine the fraction of the landscape that would be considered unstable if a given value of cohesion were present everywhere. For instance, if all soils on the landscape had a cohesion of 6 kPa, the model would predict that about 7% of our study region would fail. Figure 9d shows the fractional change in the curves of Figure 9c that occurs when the precipitation pattern is neglected. For example, if a critical cohesion threshold of 6 kPa is used, 15% fewer slopes would be identified as unstable when the uniform



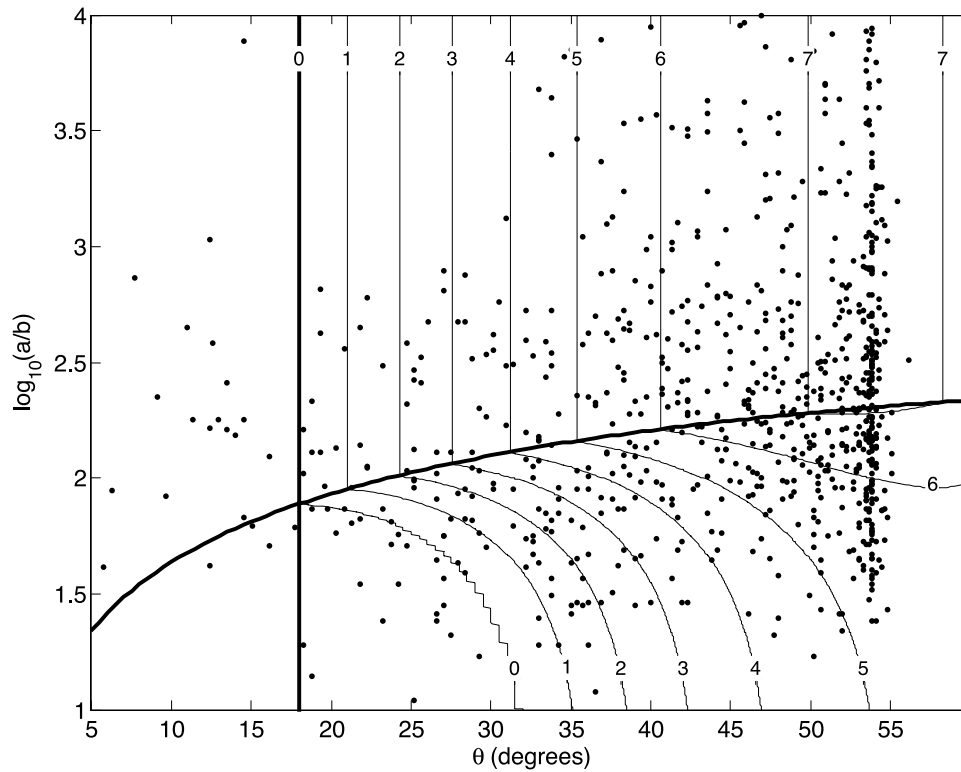


**Figure 10.** Critical cohesion (contoured and labeled every 1 kPa) as a function of  $\tan(\theta)$  and  $a/b$  using the parameters in Table 1 and uniform rainfall of 260 mm/d. The most unstable DEM grid cell in each mapped shallow slide (i.e., those shown in Figure 1) is plotted as a point on the basis of its  $\tan(\theta)$  and  $a/b$  values. Regions above the arching bold line are predicted to become saturated in the model. Locations to the left of the vertical bold line are unconditionally stable. Note that limitations of our DEM data set cause underestimation of steep slopes; thus, the slopes for points to the right of the plot are best considered as representing minimum values.

average rainfall is used instead of the rainfall pattern, indicating a significant underestimate of the area in danger of failure. When the uniform lowland rainfall is used instead of the rainfall pattern 55% fewer slopes would be identified as unstable, indicating a very substantial underestimate of the area in danger of failure. A higher (lower) percentage increases in the number of unstable slopes is found if a higher (lower)  $C_{crit}$  threshold is used, and the underestimate reaches 64% for the use of lowland rainfall when a 7 kPa is used. We thus conclude that in regions with large spatial variability in rainfall (such as the Olympic Mountains) the spatial pattern of rainfall acts to moderately increase the area prone to shallow landsliding by focusing rainfall on the mountain ridges where slopes are steep relative to the lowlands and valleys. Additionally, the use of lowland rainfall data alone to estimate hazard throughout even a relatively small mountainous catchment, may result in a substantial underestimate of the landslide susceptibility.

## 5. Sensitivity Analysis

[25] Certainly, hillslope properties that we have considered to be uniform in our analysis so far actually vary significantly on real landscapes. Even if there is a sizable effect on slope stability associated with rainfall variations, it may be largely overwhelmed by the effect of variations in other factors. We

investigate the relative importance of spatial variability in different factors by first quantifying the sensitivity of slope stability to characteristic small-scale rainfall variations, and then comparing this to the sensitivity to variations in soil properties.

[26] Figure 10 shows contours of  $C_{crit}$  predicted by SHALSTAB as a function of  $\theta$  and  $a/b$  for the parameters listed in Table 1 and uniform rainfall of 260 mm/d (roughly the mean value from the MM5 rainfall pattern). The stability of any site on the landscape may be determined by locating the point on such a plot. Note that steeper slopes lead to increased  $C_{crit}$ , as does greater topographic convergence ( $a/b$ ). However, increases in  $a/b$  only increase  $C_{crit}$  until the soil reaches saturation (this occurs along the arching bold line in Figure 10), at which point overland flow is assumed to occur and pore pressures do not increase further. The most unstable point (as predicted by value of  $C_{crit}$ ) within each mapped shallow landslide polygon is shown as a dot in Figure 10. As already shown in Figure 6, the distribution of points illustrates that while slides occur in many settings on the landscape, they are concentrated in the regions of high  $\theta$  and  $a/b$  that SHALSTAB identifies as particularly unstable.

[27] Increasing or decreasing the value of  $q$  in equation (1) by an amount characteristic of the maximum basin-scale rainfall variations ( $\pm 160$  mm/d, the difference between the maximum and minimum MM5 rainfall values) changes the

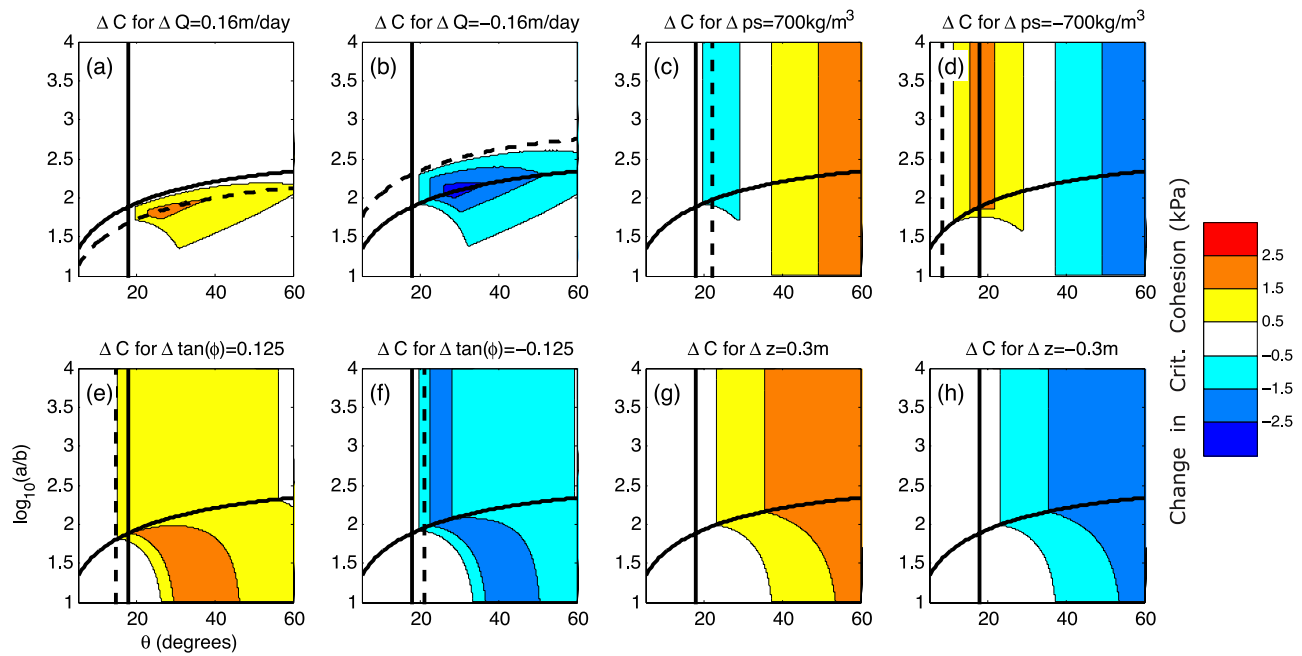


**Figure 11.** Sensitivity of  $C_{crit}$  to variations in different parameters. (a, b) Sensitivity to modeled spatial variations in rainfall ( $\pm 160$  mm/d). (c–h) Sensitivity to variations in soil parameters ( $z$ ,  $\tan\phi$ ,  $\rho_s$ ). The magnitudes of variations in soil parameters (given above the plots) are chosen to give changes in  $C_{crit}$  comparable to those due to precipitation variations shown in Figures 11a and 11b. Bold lines are thresholds as in Figure 10, and dashed lines are used to show where the thresholds move.

value of critical cohesion at each point on the landscape by the amount shown in Figures 11a and 11b. As found for our case study, changes in  $C_{crit}$  reach over 2.5 kPa. Additionally, this analysis illustrates that the sensitivity to rainfall variability is felt on a specific part of the landscape, namely near-saturated, relatively modest slopes with convergent topography, as this is where groundwater transport is focused and soils are poorly drained.

[28] Figures 11c–11h shows the analogous results for changes in three of the soil properties included in SHALSTAB ( $z$ ,  $\tan\phi$ ,  $\rho_s$ ). For comparison we choose the magnitude of changes in the soil properties so that they result in stability changes of roughly the same scale as those arising from precipitation variations in Figures 11a and 11b. Because of the form of equation (1) the sensitivity of  $C_{crit}$  to changes in both soil properties and rainfall is linear, meaning a change in any of the parameters will lead to a linearly proportional change in stability (except in regions that reach saturation or unconditional stability). Note that different regions of the landscape show sensitivity depending on which parameter is varied. For each of the soil parameters, variations of significant amplitude are required to match the effect of precipitation variations, showing that climatological patterns in extreme precipitation on the basin scale can be of comparable importance with variations in soil properties for determining the pattern of landslide hazard. The position of mapped slides on Figure 10 reveals that a significant number of slides occur in the region of large precipitation sensitivity as predicted from Figures 11a and 11b, however it is the scale of variations in precipitation relative to variations in soil properties that determines their importance in shaping the spatial distribution of hazard. For instance, Figures 10 and 11g–11h suggest that if  $\pm 30\%$  variations in soil thickness were to occur, they

would have more impact than the observed precipitation variability in the locations where most slides are found.

## 6. Conclusions

[29] We have analyzed the relationship between spatial patterns of rainfall and patterns of landslide susceptibility using high-resolution atmospheric model output (supported by gauge observations) and a physically based model of slope stability. We find that the climatological spatial variations in intense rainfall for a pair of basins in the Olympic Mountains are large enough to cause nontrivial variations in slope stability. For our study area we find that the use of area-averaged precipitation to estimate landslide susceptibility at a mountain site results in an underestimate of the area prone to failure from intense rainfall events that can exceed 20%, whereas use of lowland precipitation data can result in an underestimate of as much as 64% (Figure 9d).

[30] The destabilizing effects of the increase in precipitation from its lowland minimum to its mountain maximum may be expressed in terms of soil cohesion. In this framework we find that the enhancement of hazard at chronically rainy locations is equivalent to a substantial fraction of the actual soil cohesion supplied by vegetation in industrial and recently logged forests. This implies that the same land use produces a different level of risk in the wetter uplands than one would assume from considering lowland rainfall data and assuming spatially uniform rainfall. In particular, forestry practices that reduce root strength can carry a greater danger of slope failure in forested upland areas than in the surrounding lowlands, even for the same local slope gradients and soil properties. Furthermore, the impact of the spatial variations of rainfall observed in locations such as

the Olympic Mountains may be comparable to the effect of significant variations in soil parameters (e.g.,  $\pm 30\%$  variations in soil depth).

[31] We expect our results should generalize to a variety of regions. Similar patterns of precipitation are expected to be a common feature for midlatitude mountain ranges that receive their heaviest rainfall under convectively stable conditions. Less is known about the climatology of mountain precipitation on small scales produced by convective storms. In part because of the stochastic nature of convection, it is possible that the extreme rainfall patterns and their importance for landslide susceptibility are very different in regions that receive their heavy rainfall from such storms. As shown in Figure 11 unsaturated, relatively modest slopes with convergent topography are most sensitive to variations in rainfall, so our results are particularly pertinent for locations where many slides occur on such slopes. However, if large variations in soil properties exist, the effects of rainfall variability may be masked. Taken together, our results suggest that, for many regions, persistent spatial patterns in precipitation should be one of the factors considered in analyses of mass wasting by shallow landslides and in hazard assessments. High-resolution and high-quality data sets for mountain precipitation can be hard to come by, but strategically placed gauge networks and high-resolution atmospheric model output may prove valuable resources for the study of slope stability.

[32] **Acknowledgments.** We thank Cliff Mass's research group at the University of Washington for providing the MM5 model output and Neil Johnson for assistance in dearchiving it. Harvey Greenberg provided substantial technical assistance in the GIS analysis. The work also benefited from conversations with Bill Dietrich and his research group. J.R.M. received support from a National Science Foundation (NSF) Graduate Research Fellowship. The work was also supported by NSF grant (EAR-0642835).

## References

- Anders, A. M., G. H. Roe, B. Hallet, D. R. Montgomery, N. Finnegan, and J. Putkonen (2006), Spatial patterns of precipitation and topography in the Himalaya, in *Tectonics, Climate, and Landscape Evolution*, edited by S. Willett et al., *Geol. Soc. Am. Spec. Pap.*, 398, 39–53.
- Anders, A. M., G. H. Roe, D. R. Durran, and J. R. Minder (2007), Small-scale spatial gradients in climatological precipitation on the Olympic Peninsula, *J. Hydrometeorol.*, 8(5), 1068–1081.
- Baeza, C., and J. Corominas (2001), Assessment of shallow landslide susceptibility by means of multivariate statistical techniques, *Earth Surf. Processes Landforms*, 26(12), 1251–1263.
- Bergeron, T. (1968), On the low-level distribution of atmospheric water caused by orography, in *Proceedings of the International Conference on Cloud Physics*, pp. 96–100, Int. Assoc. of Meteorol. and Atmos. Phys., Toronto, Ont., Canada.
- Caine, N. (1980), The rainfall intensity-duration control of shallow landslides and debris flows, *Geogr. Ann., Ser. A*, 62(1), 23–27.
- Campbell, R. (1975), Soil slips, debris flows, and rainstorms in the Santa Monica Mountains and vicinity, southern California, *U.S. Geol. Surv. Open File*, pp. 75–851.
- Casadel, M., W. E. Dietrich, and N. L. Miller (2003), Testing a model for predicting the timing and location of shallow landslide initiation in soil-mantled landscapes, *Earth Surf. Processes Landforms*, 28(9), 925–950.
- Chang, K. T., S. H. Chiang, and F. Lei (2008), Analysing the relationship between typhoon-triggered landslides and critical rainfall conditions, *Earth Surf. Processes Landforms*, 33(8), 1261–1271.
- Gorsevski, P. V., P. E. Gessler, J. Boll, W. J. Elliot, and R. B. Foltz (2006), Spatially and temporally distributed modeling of landslide susceptibility, *Geomorphology*, 80(3–4), 178–198.
- Groisman, P. Y., and D. R. Legates (1994), The accuracy of United States precipitation data, *Bull. Am. Meteorol. Soc.*, 75(2), 215–227.
- Gupta, R., and B. Joshi (1990), Landslide hazard zoning using the GIS approach—A case-study from the Ramganga catchment, Himalayas, *Eng. Geol.*, 28(1–2), 119–131.
- Guzzetti, F., S. Peruccacci, M. Rossi, and C. P. Stark (2008), The rainfall intensity-duration control of shallow landslides and debris flows: An update, *Landslides*, 5(1), 3–17.
- Hong, Y., R. Adler, and G. Huffman (2006), Evaluation of the potential of NASA multi-satellite precipitation analysis in global landslide hazard assessment, *Geophys. Res. Lett.*, 33, L22402, doi:10.1029/2006GL028010.
- Iverson, R. M. (2000), Landslide triggering by rain infiltration, *Water Resour. Res.*, 36(7), 1897–1910.
- James, C., and R. Houze (2005), Modification of precipitation by coastal orography in storms crossing northern California, *Mon. Weather Rev.*, 133(11), 3110–3130.
- Kirshbaum, D. J., and D. R. Durran (2005), Observations and modeling of banded orographic convection, *J. Atmos. Sci.*, 62(5), 1463–1479.
- Lee, S. J., H. Ryu, K. D. Min, and J. S. Won (2003), Landslide susceptibility analysis using GIS and artificial neural network, *Earth Surf. Processes Landforms*, 28(12), 1361–1376.
- Lingey, L. (1999), Geology, in *Quinault River Watershed Analysis: Quinault Indian Nation*, vol. 1, chap. 2, pp. 2.3.1–2.3.27, Quinault Indian Nation, Taholah, Wash.
- MacLeod, A. (2006), Coupling meteorological data with hydrologic and slope stability models to constrain controls on shallow landsliding, M.S. thesis, Univ. of Oreg., Eugene.
- Mass, C. F., et al. (2003), Regional environmental prediction over the Pacific Northwest, *Bull. Am. Meteorol. Soc.*, 84(10), 1353–1366.
- Minder, J., D. Durran, G. Roe, and A. Anders (2008), The climatology of small-scale orographic precipitation over the Olympic Mountains: Patterns and processes, *Q. J. R. Meteorol. Soc.*, 134(633), 817–839.
- Montgomery, D. R., and W. E. Dietrich (1994), A physically based model for the topographic control on shallow landsliding, *Water Resour. Res.*, 30(4), 1153–1171.
- Montgomery, D. R., K. Sullivan, and H. M. Greenberg (1998), Regional test of a model for shallow landsliding, *Hydrol. Processes*, 12(6), 943–955.
- Montgomery, D. R., K. M. Schmidt, H. M. Greenberg, and W. E. Dietrich (2000), Forest clearing and regional landsliding, *Geology*, 28(4), 311–314.
- Morrissey, M., G. Wiczorek, and B. Morgan (2004), Transient hazard model using radar data for predicting debris flows in Madison County, Virginia, *Environ. Eng. Geosci.*, 10(4), 285–296.
- Pike, R. J., and S. Sobieszcyk (2008), Soil slip/debris flow localized by site attributes and wind-driven rain in the San Francisco Bay region storm of January 1982, *Geomorphology*, 94(3–4), 290–313.
- Roe, G. H. (2005), Orographic precipitation, *Annu. Rev. Earth Planet. Sci.*, 33, 645–671.
- Saha, A. K., R. P. Gupta, I. Sarkar, M. K. Arora, and E. Csaplovics (2005), An approach for GIS-based statistical landslide susceptibility zonation—With a case study in the Himalayas, *Landslides*, 2(1), 61–69.
- Schmidt, J., G. Turek, M. P. Clark, M. Uddstrom, and J. R. Dymond (2008), Probabilistic forecasting of shallow, rainfall-triggered landslides using real-time numerical weather predictions, *Nat. Hazards Earth Syst. Sci.*, 8(2), 349–357.
- Schmidt, K. M., J. J. Roering, J. D. Stock, W. E. Dietrich, D. R. Montgomery, and T. Schaub (2001), The variability of root cohesion as an influence on shallow landslide susceptibility in the Oregon Coast Range, *Can. Geotech. J.*, 38(5), 995–1024.
- Smith, R. B., Q. F. Jiang, M. G. Fearon, P. Tabary, M. Dorninger, J. D. Doyle, and R. Benoit (2003), Orographic precipitation and air mass transformation: An Alpine example, *Q. J. R. Meteorol. Soc.*, 129(588), 433–454.
- Wiczorek, G. F., H. McWreath, and C. Davenport (2001), Remote rainfall sensing for landslide hazard analysis, *U.S. Geol. Surv. Open File Rep.*, 01-339.
- Wu, W., and R. C. Sidle (1995), A distributed slope stability model for steep forested basins, *Water Resour. Res.*, 31(8), 2097–2110.

J. R. Minder, Department of Atmospheric Sciences, University of Washington, Box 351640, Seattle, WA 98195-1640, USA. (juminder@atmos.washington.edu)

D. R. Montgomery and G. H. Roe, Department of Earth and Space Sciences, University of Washington, Seattle, WA 98195-1310, USA.